THE JOURNAL OF PHYSICAL CHEMISTRY B

ARTICLE

pubs.acs.org/JPCB

UV Resonance Raman Studies of the $NaClO_4$ Dependence of Poly-L-lysine Conformation and Hydrogen Exchange Kinetics

Lu Ma, Zhenmin Hong, Bhavya Sharma, and Sanford Asher*

Department of Chemistry, University of Pittsburgh, Pittsburgh, Pennsylvania 15260, United States

ABSTRACT: We used 204 nm excitation UV Resonance Raman (UVRR) spectroscopy to examine the effects of $NaClO_4$ on the conformation of poly-L-lysine (PLL). The presence of $NaClO_4$ induces the formation of α-helix, π-helix/bulge, and turn conformations. The dependence of the $AmIII_3$ frequency on the peptide Ψ Ramachandran angle allows us to experimentally determine the conformational population distributions and the energy landscape of PLL along the Ramachandran Ψ angle. We also used UVRR to measure the $NaClO_4$ concentration dependence of PLL amide hydrogen exchange kinetics. Exchange rates were determined by fitting the D_2O exchanging PLL UVRR AmII′ band time evolution. Hydrogen exchange is slowed at high $NaClO_4$ concentrations. The PLL AmII′ band exchange kinetics at 0.0, 0.2, and 0.35 M $NaClO_4$ can be fit by single exponentials, but the AmII′ band kinetics of PLL at 0.8 M $NaClO_4$ requires a double exponential fit. The exchange rates for the extended conformations were monitored by measuring the C_α−H band kinetics. These kinetics are identical to those of the AmII′ band until 0.8 M $NaClO_4$ whereupon the extended conformation exchange becomes clearly faster than that of the α-helix-like conformations. Our results indicate that ClO_4^- binds to the PLL backbone to protect it from OH^- exchange catalysis. In addition, ClO_4^- binding also slows the conformational exchange between the extended and α-helix-like conformations, probably by increasing the activation barriers for conformational interchanges.

$NaClO_4$ decreases PLL D/H and conformational exchange rates

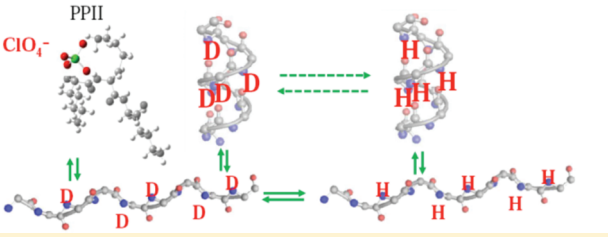

INTRODUCTION

An understanding of the mechanism(s) of protein folding remains an important unsolved problem in structural biology.[1−6] The major underlying assumption is that the protein native structure is the most thermodynamically stable structure.[7−9] Thus, the protein primary sequence is expected to contain all of the information necessary to specify both the protein native structure and its folding mechanism(s). The well-known Levinthal paradox implies that there exist specific folding intermediates or pathways through which the protein quickly evolves into its final functional structure.[10]

The mechanisms of protein folding have been probed experimentally by techniques such as CD, NMR, IR, Raman, fluorescence, and a variety of time-resolved spectroscopies, mutational studies, and hydrogen exchange methods.[11−16] Most recently, single-molecule methods have probed the distributions of the unfolded and folded states by following the folding reaction of individual molecules.[17−20] Single-molecule methods, such as optical tweezers and AFM, have been used to elucidate protein folding intermediates and the energy landscapes by using mechanical force as a denaturant.[17,21] Computational modeling has also made significant contributions to the understanding of protein folding.[22−24]

In the work here, we use UV resonance Raman (UVRR) spectroscopy to study the conformational distributions of poly-L-lysine (PLL) in the presence of different $NaClO_4$ concentrations. ClO_4^- induces an α-helix conformation at neutral and low pH values, where the lysine side chains are positively charged.[25,26] Ma et al. recently observed that PLL adopts multiple α-helix-like conformations in the presence of ClO_4^-, including pure α-helix and π-bulge/helix conformations.[27]

We also determined the dependence of the PLL conformational population distributions and the energy landscapes on $NaClO_4$ concentration. We measured the hydrogen exchange behavior of the PLL peptide bond NH at pH 2.8 at different $NaClO_4$ concentrations. The results show that the exchange rates are $NaClO_4$ concentration dependent and that the hydrogen exchange behavior indicates that the PLL conformations are in rapid equilibrium until the highest $NaClO_4$ concentrations where two exchange rates are observed.

EXPERIMENTAL SECTION

Materials. Poly-L-lysine HCl (MW_{vis} = 20 900, DP_{vis}= 127, MW_{MALLS} = 11 400, DP_{MALLS} = 69, where DP_{vis} and DP_{MALLS} refer to the degree of polymerization measured by viscosity and multiangle laser light scattering, respectively) was obtained from Sigma Co. and used without further purification. $NaClO_4$ was purchased from Sigma Co. and was used without further purification. D_2O (99.9 atom % D) was purchased from Cambridge Isotope Laboratories, Inc. Small aliquots of HCl and DCl solutions were used to adjust the solution pH values. DCl

Received: September 15, 2011
Revised: November 11, 2011
Published: November 26, 2011

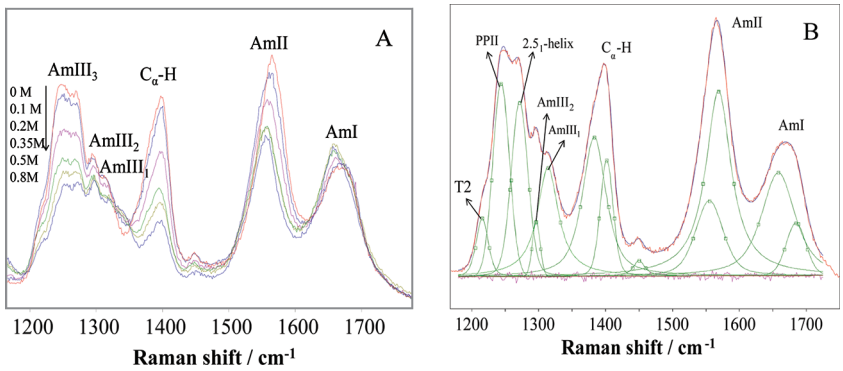

Figure 1. (A) UVRR spectra (204 nm) of PLL at pH 3 and 20 °C at 0, 0.1, 0.2, 0.35, 0.5, and 0.8 M $NaClO_4$ concentrations. (B) Deconvolution of the 20 °C 204 nm UVRR PLL spectrum in the absence of $NaClO_4$ at pH 3.

(99 + atom % D) was acquired from Aldrich. The UVRR spectra of PLL at different $NaClO_4$ concentrations were measured at 0.85 mg/mL peptide concentrations at pH 3, and the spectra were normalized to the Raman intensity of the symmetric stretching band of ClO_4^-.

UVRR Instrument. We used a Coherent Infinity Nd:YAG laser (Coherent, Inc.) to produce 355 nm light pulses (third harmonic) at a 100 Hz repetition rate with a pulse width of 3 ns. This beam was Raman shifted to 204 nm (fifth anti-Stokes) using a 1 m tube filled with hydrogen (60 psi), giving 2 mW average power.[28,29] A Pellin Broca prism was used to select the 204 nm excitation. The sample was circulated in a free surface, temperature-controlled stream to avoid heating or accumulation of photochemical degradation products formed by the high peak power laser pulses. The Raman scattered light was imaged into a subtractive double spectrometer.[28] The dispersed UV light was detected by the liquid nitrogen cooled, Unichrome coated, back-thinned CCD with a >30% quantum efficiency in the deep UV (Princeton Instruments Spec−10:400B). More details on the UVRR apparatus are given by Bykov et al.[28]

CD Measurements. Circular dichroism (CD) spectra were measured by using a Jasco J-710 spectropolarimeter. The spectra were measured by using a temperature-controlled 0.2 mm path length cell with 0.87 mg/mL PLL concentrations.

Hydrogen Exchange Experiment. pD 2.9 D_2O solutions (1 mL) containing 8.5 mg of PLL and 0, 0.2, 0.35, or 0.8 M $NaClO_4$ concentrations were prepared and mixed rapidly with a 9 mL H_2O solution at pH 2.8 with the same $NaClO_4$ concentrations. The dead times for all mixing experiments were 25−60 s. The time-dependent UVRR spectra of the solutions at 0.85 mg/mL PLL concentration containing 0, 0.2, 0.35, or 0.8 M $NaClO_4$ were collected at 5 s intervals with 5 s data accumulation times. For samples containing $NaClO_4$, all Raman spectra are normalized to the intensity of the 932 cm^{-1} ClO_4^- Raman band. In the absence of $NaClO_4$, the AmI (AmI′) band intensity was used as the internal intensity standard.

RESULTS AND DISCUSSION

$NaClO_4$ Dependence of 204 nm UVRR Spectra of PLL. Previous studies show that $NaClO_4$ converts unfolded PLL with charged side chains to α-helix-like conformations.[27] For example, 0.8 M $NaClO_4$ at pH 5.5 at 2.5 °C converts normally extended PLL conformations to an ∼86% α-helix-like content.[30] Figure 1A shows the 204 nm UVRR spectra of PLL at different $NaClO_4$ concentrations at pH 3 and 20 °C. In the absence of $NaClO_4$, as observed previously, PLL occurs in an equilibrium between extended polyproline II (PPII) and 2.5_1-helix conformations at low pH.[27,31] These conformations give rise to $AmIII_3$ bands at ∼1245 and ∼1268 cm^{-1}, respectively, as shown in Figure 1B. As the $NaClO_4$ concentration increases the intensities of the AmIII bands between 1190 and 1300 cm^{-1}, the ∼1400 cm^{-1} C_α−H b band and the ∼1567 cm^{-1} AmII band decrease. In addition, the AmI and AmII band frequencies downshift; 0.8 M $NaClO_4$ causes the AmI and AmII bands to downshift by 12 cm^{-1}, and the AmI band shape narrows and becomes more symmetric. These spectral changes indicate the formation of α-helical-like conformations as confirmed by the CD measurements in Figure 2.

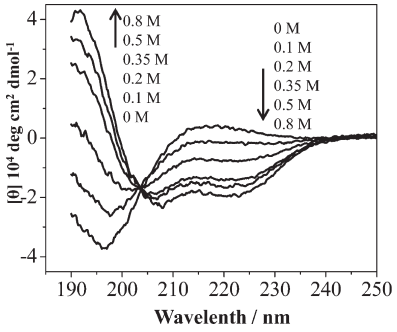

Figure 2. $NaClO_4$ concentration dependence of 0.87 mg/mL of PLL CD spectra at pH 3 and 20 °C.

We previously believed that $NaClO_4$ converts charged PLL to a highly α-helical conformation by forming ion pairs between ClO_4^- and the PLL $-NH_3^+$ side chains to neutralize the repulsions that destabilize α-helical conformations.[27,32−34] A simple Debye−Hückel screening mechanism was excluded because high NaCl concentrations negligibly impact the PLL conformation.[26,30] Ion-pair formation should dramatically decrease side chain electrostatic repulsions. This should decrease the 2.5_1-helix conformation content that is stabilized by side chain electrostatic repulsions.

Indeed, our previous study of K10 (Ac−lys10−NH_2) demonstrated that the neutralization of the charged lysine side chains at increased pH significantly decreased the relative fraction of 2.5_1-helix compared to that of the PPII conformation.[30] However, surprisingly, the UVRR spectra of PLL showed that $NaClO_4$ does not decrease the relative fraction of 2.5_1-helix significantly

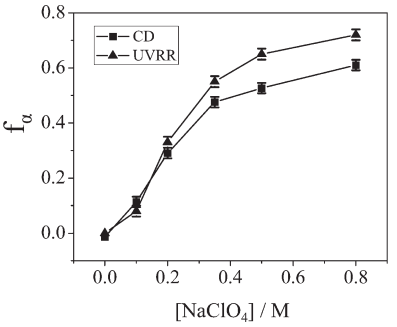

Figure 3. Comparison of the PLL α-helix-like conformation fraction calculated from CD and UVRR at different $NaClO_4$ concentrations at pH 3 and 20 °C.

compared to that of the PPII conformation. We frankly do not understand this result.

The C_α−H b bands that are resonantly enhanced in the extended PPII, β-sheet, and β-strand-like conformations are not enhanced in the α-helix-like conformations. As a result, in Figure 1A, the C_α−H b band shows a large intensity decrease relative to that of the AmII and AmIII bands. Using the C_α−H b band intensity to indicate the extended PLL concentration content, we subtract the appropriate amount of the extended PLL spectrum from the measured spectra, leaving the UVRR of the $NaClO_4$-induced α-helix conformation. This subtraction assumes that the extended conformation possesses an invariant UVRR spectrum as the $NaClO_4$ concentration increases; this assumption is supported by the fact that the UVRR difference spectra between successive additions of $NaClO_4$ are very similar and that the system appears to be two state from the Figure 1 and Figure 2 isosbestic points in the UVRR and the CD.

Figure 3 shows the estimated α-helix-like fraction of PLL at different $NaClO_4$ concentrations obtained from the UVRR. The α-helix-like content fraction of PLL at different $NaClO_4$ concentrations, f_H, can also be calculated from the Figure 2 CD spectra by utilizing the equation[29,35]

$$f_H = \frac{\theta_{222} - \theta_r}{\theta_H - \theta_r} \quad (1)$$

θ_{222} is the molar ellipticity at 222 nm, which is assumed to be proportional to the α-helix content, and θ_r and θ_H are the molar ellipticities of the extended and α-helix-like conformations. Here, θ_r was experimentally measured as 2854 deg cm^2 dmol^{-1}, and θ_H = 32 200 deg cm^2 dmol^{-1} is the mean residue ellipticity as averaged over several polypeptides.[36]

The α-helix-like fraction obtained from CD is smaller than that obtained from UVRR (Figure 3). The 222 nm CD ellipticity results from interpeptide bond exciton coupling of the α-helical conformation electronic dipole transition moments. The ellipticity per residue decreases for short α-helices.[29,35,37]

In contrast, the Raman intensity is the sum of the intensities from each peptide bond. We calculated the α-helix fraction by assuming that there only exist two conformations, either an extended conformation or an α-helix-like conformation. We used the C_α−H b band intensity to calculate the PLL extended conformational fraction. We do not expect phenomena such as hypochromism to alter the extended conformation peptide bond Raman cross sections.

We calculated the UVRR α-helix-like conformation fraction from $f_H = 1 - f_{extended}$. The α-helix-like conformational fractions

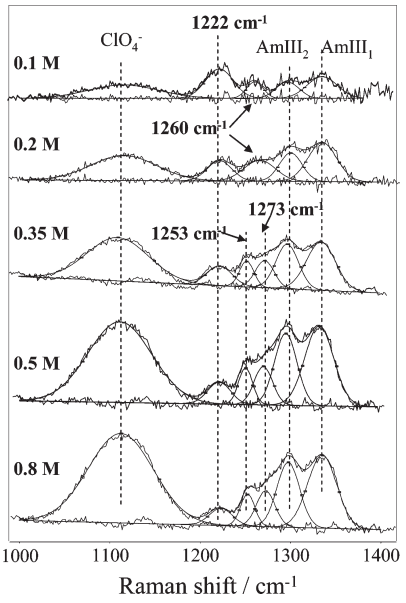

Figure 4. $NaClO_4$ concentration dependence of the AmIII region of the 204 nm UVRR spectra of the calculated α-helix-like PLL conformations at pH 3 and 20 °C. See text for details.

calculated from the UVRR include α-helix-like turns that do not give significant contributions to the 222 nm ellipticity. Thus, the Raman indicates a higher α-helix-like fraction than CD (Figure 3).

Figure 4 shows the calculated α-helix-like PLL AmIII region UVRR spectra. The AmIII region of the α-helix-like PLL spectra is well modeled by Gaussian bands. The 1110 cm^{-1} band derives from the ClO_4^- asymmetric stretching band, while the AmIII$_1$ and AmIII$_2$ bands are located at 1332 and 1294 cm^{-1}. As shown in Figure 4 the AmIII$_3$ band spectral region depends on the $NaClO_4$ concentration. At 0.1 and 0.2 M $NaClO_4$ concentrations, the AmIII$_3$ region resolves into two bands at 1222 and 1260 cm^{-1}. In contrast, at 0.35, 0.5, and 0.8 M $NaClO_4$, the AmIII$_3$ region resolves into three bands at 1222, 1253, and 1273 cm^{-1}.

$NaClO_4$ Dependence of PLL Ψ Angle Distribution. Using the method developed by Mikhonin et al,[38] we can calculate the Ramachandran Ψ angle distribution from the AmIII$_3$ band frequency distribution if we know the peptide bond hydrogen bonding states.[38−40] Figure 5 shows the $NaClO_4$ concentration dependence of the Ψ angle distributions of PLL calculated from the AmIII$_3$ bands deriving from the calculated α-helix-like spectra of Figure 4 and from the pure extended conformations of PLL in the absence of $NaClO_4$ of Figure 1B.

Assuming α-helix-like intramolecular peptide bond hydrogen bonding, the 1273, 1260, and 1253 cm^{-1} AmIII$_3$ bands are calculated to derive from conformations with average Ramanchandran Ψ angles of −60°, −43°, and −36°.[38]

Thus, the 1273 and 1253 cm^{-1} AmIII$_3$ bands derive from π-bulge and pure α-helix conformations, respectively. The 1260 cm^{-1} AmIII$_3$ band occurs at a frequency between that of the α-helix and π-bulge/helix conformation. It could derive from distorted α-helix or π-helix conformations.

The 1222 cm^{-1} AmIII$_3$ band could result from Ψ angles, of either 4° or 124°. Because the 1222 cm^{-1} AmIII$_3$ band does not also show the significant intensity in the C_α−H b band region that would be expected for this partially extended structure, we

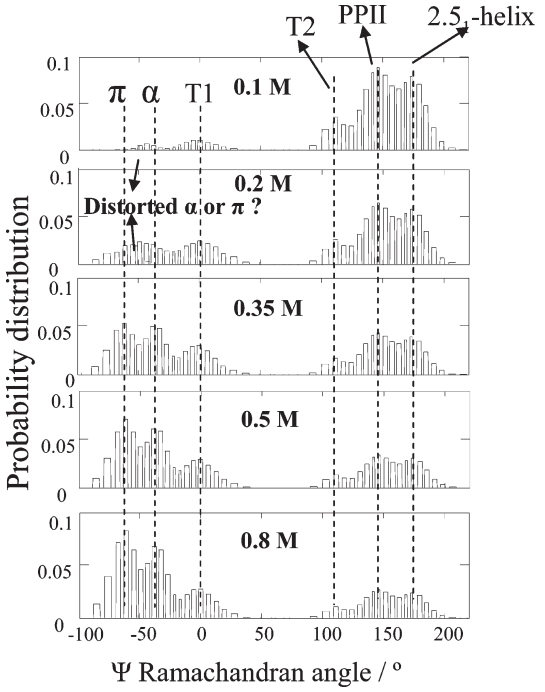

Figure 5. $NaClO_4$ concentration dependence of the Ramachandran Ψ angle distributions of PLL at pH 3 and 20 °C, assuming the T2 conformation at Ψ = 114°. The possible Ψ = 14° conformation is not shown. The extended structure Ψ angles are assumed to be those of PLL in the absence of $NaClO_4$ as in Figure 1B.

exclude the 124° Ψ angle possibility and assume that the conformation is close to that of an α-helix. This conformation could derive from type I or I′ and type II or II′ turns from their i+2 residues based on this Ψ value.[38] For brevity we label this turn conformation T1. We assume here equal Raman cross sections for α-helix, π-helix, and T1 structures.

The extended conformation PLL spectra, measured in the absence of $NaClO_4$, shown in Figure 1B show three $AmIII_3$ bands. Two were assigned to the PPII and 2.5$_1$-helix conformations, as discussed above. The third $AmIII_3$ band appears as a shoulder at 1214 cm^{-1}. This band which we label T2 could also result from turn conformations, with Ψ angles of either 14° or 114°. However, it is unclear whether this turn conformation shows significant C_α−H b band intensity because of the overwhelming contributions of the PPII and 2.5$_1$-helix conformations.

Ψ = 14° could derive from a somewhat distorted type I, II, or II′, i+2 residues, or type I′ or III′, i+1 and i+2 residues. Ψ = 114° could derive from a somewhat distorted type II, i+1 residues, or a type VIII, i+2 residue.[38] Figure 5 shows the Ψ distribution assuming that the T2 conformation possesses Ψ = 114° and that this conformation shows Raman bands with the same cross sections as the PPII and 2.5$_1$-helix extended conformations.

At 0.1 M $NaClO_4$, the Ψ angle distribution shows only the distorted α-helix or π-bulge conformations and the T1 and T2 turn structures and the PPII and 2.5$_1$-helix structures. π-Bulge structures are induced by increasing the $NaClO_4$ concentration. Further, as the $NaClO_4$ concentration increases, the α-helix-like content increases, decreasing the extended conformation content. The relative concentrations of α-helix and π-bulge concentrations increase compared to that of the T1 turn structure.

Conformational Free Energy Landscapes of PLL. We can use the calculated conformation population distribution of Figure 5 to calculate the Gibbs free energy of the equilibrium conformations relative to the PPII conformation along the Ψ Ramachandran angle folding reaction coordinate.[27,31] Figure 6 shows the resulting energy landscapes at different $NaClO_4$ concentrations at pH 3 and 20 °C. The energy landscapes contain an α-helix-like conformational basin and an extended conformation energy basin.

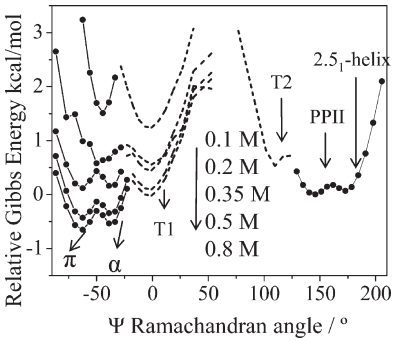

Figure 6. Calculated Gibbs free energy landscapes for PLL at different $NaClO_4$ concentrations at pH 3 and 20 °C. The dotted lines show the turn regions, assuming that the T2 turn occurs at Ψ =114°.

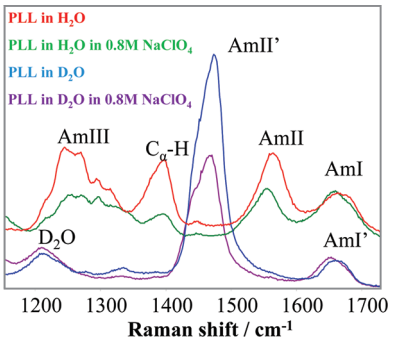

Figure 7. UVRR spectra (204 nm) of PLL in the absence and presence of 0.8 M $NaClO_4$ in H_2O and D_2O at pH 3/pD 3 and at 20 °C.

At 0.1 M $NaClO_4$, the α-helical basin shows a double well with a separate minima from the α-helix and the T1 turn structure. The α-helix and π-bulge conformations lie 1.5 kcal/mol above those of the PPII and 2.5$_1$-helix conformations. Increasing the $NaClO_4$ concentration lowers the α-helix-like conformation basin energy. At 0.2 M $NaClO_4$, the α-helix-like conformation is 0.58 kcal/mol above the PPII and 2.5$_1$-helix conformations. At 0.35 M $NaClO_4$, the α-helix or π-helix-like energy well splits into an α-helix, π-bulge, and T1 triplet of energy minima. The α-helix, π-bulge, and T1 triplet energies are similar to those of the PPII and 2.5$_1$-helix conformations. At 0.8 M $NaClO_4$, the α-helix and π-bulge conformational energies are 0.55 and 0.65 kcal/mol below that of extended conformations, consistent with our previous study.[27] The relative energy of the T1 conformation energy decreases less than that of the α-helix and π-bulge conformations. The variations in shape of the PLL Gibbs free energy landscapes with changing $NaClO_4$ concentration indicate that complex conformation changes occur as the $NaClO_4$ concentration increases.

UVRR Spectra of Protonated and Deuterated PLL. Deuteration of the PLL backbone N−H groups leads to significant PLL UVRR spectral changes[30] because the AmII, AmIII, and C_α−H b bands involve significant N−H bending; deuteration

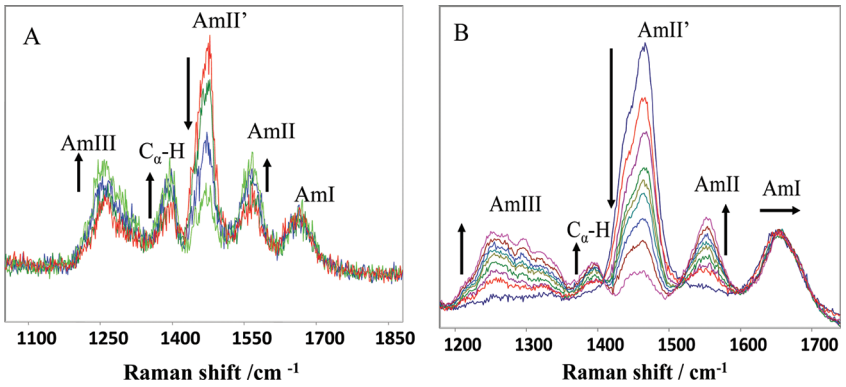

Figure 8. (A) pH 2.8 UVRR of PLL at 20 °C hydrogen exchange at 28, 33, 43, and 103 s after H_2O addition in the absence of $NaClO_4$. (B) pH 2.8 UVRR PLL hydrogen exchange in 0.8 M $NaClO_4$ obtained at 3, 8, 12, 22, 32, 42, 64, 102, and 150 min after 0.8 M $NaClO_4$ H_2O solution addition.

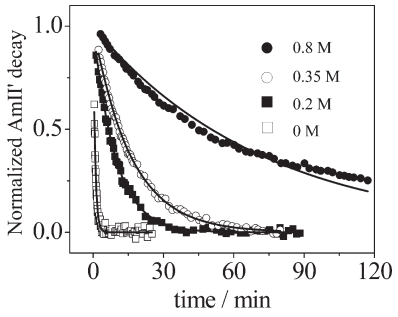

Figure 9. Time dependence of normalized AmII′ band intensity of PLL due to H exchange at pH 2.8 at 20 °C at different $NaClO_4$ concentrations. The thin solid lines show single exponential fitting.

removes the N−H in plane bending component, leaving an almost pure C−N s AmII′ vibration at 1470 cm^{-1} and an AmIII′ vibration at 935 cm^{-1} which has a large N−D bending component. Figure 7 shows the pH 3 UVRR spectrum of PLL in the absence and presence of 0.8 M $NaClO_4$ in H_2O and D_2O. In D_2O the AmIII, AmII, and C_α−H b bands disappear and are replaced with the very strong AmII′ band and a weak AmIII′ band (not shown). The UVRR spectra clearly differentiate between ND vs NH peptide bonds. The AmII′ band is strong and well resolved, allowing for accurate quantitative analysis of the relative deuterated fraction.

$NaClO_4$ Dependence of PLL Amide Hydrogen Exchange Rate. We examined PLL hydrogen exchange at 0, 0.2, 0.35, and 0.8 M $NaClO_4$ concentrations, by mixing PLL D_2O $NaClO_4$ solutions rapidly with H_2O $NaClO_4$ solutions. Figure 8 shows the evolution of the UVRR on hydrogen exchange of PLL in the absence and presence of 0.8 M $NaClO_4$. The AmII′ band gradually loses intensity upon replacement of N−D by N−H, while the AmII, C_α−H b, and AmIII bands gain intensity.

Figure 9 shows the normalized intensity decay of the AmII′ band calculated as

$$I_{N,\,AmII'}(t) = \frac{I_{AmII'}(t) - I_{AmII'}(\infty)}{I_{AmII'}(0) - I_{AmII'}(\infty)} \qquad (2)$$

where $I_{N,AmII'}(t)$ is the normalized AmII′ intensity decay, whose value decreases from 1.0 to 0.0; $I_{AmII'}(t)$ is the experimentally observed AmII′ band intensity at exchange time t; and $I_{AmII'}(0)$ and $I_{AmII'}(\infty)$ are the AmII′ band intensities at $t = 0$ and $t = \infty$. Since the AmII′ band shapes at all exchange times for specific $NaClO_4$ concentration are almost identical, we utilized peak height intensities for analysis.

The 1459 cm^{-1} HOD bending band partially overlaps the AmII′ band. Since the H_2O/D_2O rapidly reaches equilibrium, the HOD bending band contribution to the AmII′ band intensity is constant at all times during the PLL hydrogen exchange. Thus, the HOD band subtracts off during the data analysis using eq 2.

As the $NaClO_4$ concentration increases, hydrogen exchange slows (Figure 9). The apparent exchange rate is calculated by fitting the normalized AmII′ band intensities. The AmII′ intensity decay curves at 0, 0.2, and 0.35 M $NaClO_4$ concentrations at pH 2.8 are well fit by single exponentials with apparent exchange rates of 0.95, 0.11, and 0.063 min^{-1}, respectively. The best single exponential fitting to the AmII′ 0.8 M exchange curve gave an apparent exchange rate of 0.014 min^{-1}. However, Figure 9 shows that the 0.8 M exchange curve does not fit well to a single exponential. Excellent fitting was obtained with a double exponential that gives apparent rates of 0.022 and 0.00097 min^{-1} with weighting factors of 0.77 and 0.23 for the two exponents, respectively, as discussed below.

We also monitored the normalized intensity increase upon exchange that occurs for the C_α−H b band ($I_{N,C-H}(t) = (I_{C-H}(t) - I_{C-H}(0))/(I_{C-H}(\infty) - I_{C-H}(0))$) that is plotted together with $1-I_{N,AmII'}(t)$ in Figure 10. At 0.0, 0.2, and 0.35 M $NaClO_4$ concentrations, the AmII′ and C_α−H b band kinetics fully overlap.

We also monitored the normalized intensities of the 1567 cm^{-1} AmII band and the 1250 and 1267 cm^{-1} components of the $AmIII_3$ band. At 0.0, 0.2, and 0.35 M $NaClO_4$ concentrations, the AmII and the $AmIII_3$ band kinetics overlap those of the AmII′ band. However, at 0.8 M $NaClO_4$, the $I_{N,C-H}(t)$ kinetics are faster than that of $1-I_{N,AmII'}(t)$ as shown in Figure 10. The AmII band kinetics is very close to that of the AmII′ band, while the 1250 and 1267 cm^{-1} $AmIII_3$ band kinetics fall between the $I_{N,C-H}(t)$ and $1-I_{N,AmII'}(t)$ kinetics (not shown).

In the presence of $NaClO_4$, PLL has multiple conformations in equilibrium (α, π, turn, PPII, 2.5_1-helix, etc.). All conformations with NH peptide bonds contribute to the AmII and AmIII bands, with the α-helical-like conformations contributing with lower Raman cross sections. Uniquely, the C_α−H b band is contributed only by NH peptide bond extended conformations. All ND peptide bonds contribute to the AmII′ band, with the α-helical conformation showing a lower Raman cross section.

The exchange rates of the peptide bond NH in the extended conformations can be selectively calculated from the C_α−H b

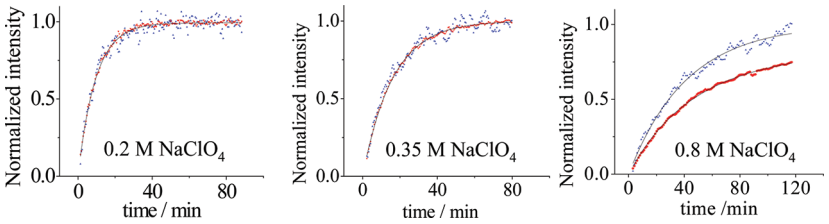

Figure 10. Comparison of $I_{N,C-H}(t)$ (blue) and $1-I_{N,AmII'}(t)$ (red) exchange kinetics of the $C_\alpha-H$ b band and AmII′ band at pH 2.8 at 20 °C. The black lines are single exponential (0.2, 0.35 M) and double exponential (0.8 M) fitting curves.

band exchange kinetics shown in Figure 10. At 0.0, 0.2, and 0.35 M, identical exchange rates are observed for the $C_\alpha-H$ b band from the extended structure, as from the AmII′ band contributed by the predominant α-helix conformation. In sharp contrast, in 0.8 M $NaClO_4$, the extended conformation monitored 0.024 min^{-1} single exponential $C_\alpha-H$ b band calculated exchange rate is almost twice as fast as that of the mainly α-helix AmII′ band of 0.014 min^{-1}. As discussed above, the hydrogen exchange rates of the peptide bond NH in the extended conformations slow as the $NaClO_4$ concentration increases. The AmII and AmIII monitored D/H exchange kinetics show a poorer S/N because the magnitude of the spectral changes is attenuated by the overlapping slow α-helix exchange rates and by the weaker, broader AmIII bands that contain partially overlapping contributions of α-helix-like and extended conformations.

The H/D exchange rates for PLL in solution should follow the scheme:

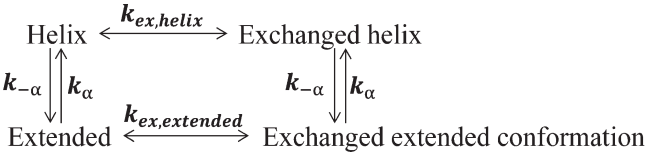

where "Helix" and "Extended" represent the α-helix-like and extended conformations; $k_{ex,helix}$ and $k_{ex,extended}$ refer to the H/D exchange rate constants of the peptide bond NH in the α-helix-like and extended conformations, respectively; k_α and $k_{-\alpha}$ are rate constants for the conformational transformation between the α-helix-like and extended conformations; and the equilibrium constant $K = k_{-\alpha}/k_\alpha = [\text{extended}]/[\text{helix}]$. At 0.0 M $NaClO_4$, only the extended conformation exists. At 0.2, 0.35, and 0.8 M $NaClO_4$, $K = k_{-\alpha}/k_\alpha$ can be calculated to be 2.0, 0.82, and 0.39, respectively.

The overlapping time dependencies of the normalized intensities of the AmII′, $C_\alpha-H$ b, AmII, and the 1250, 1267 cm^{-1} $AmIII_3$ band kinetics for 0.2 and 0.35 M $NaClO_4$ concentrations indicate that either the hydrogen exchange rates for the extended and α-helix-like conformations are identical or the conformational interconversion rate is significantly faster than our H/D exchange measurement time scale. Since we expect the α-helix-like conformation to have a very slow D/H rate, we must conclude that we are actually monitoring the D/H exchange of the extended conformation and that conformational exchange is very fast between the α-helix-like conformation and extended conformations.

However, the 0.8 M $NaClO_4$ solution PLL sample of Figure 10 shows faster kinetics for the extended conformation $C_\alpha-H$ b band than for the predominantly α-helix AmII′ band, indicating that the extended structure undergoes D/H exchange faster than the α-helix, *and* that the conformational interconversion rates are slow compared to the D/H exchange rates.

Thus, the conformational interconversion rate of PLL decreases as the $NaClO_4$ concentration increases. ClO_4^- binding probably increases the activation barriers restricting the conformational interconversion rate. Previous studies showed that peptide conformational dynamics could be influenced by the presence of salts.[41] Further, Dzubiella et al. MD simulations showed that the α-helical (un)folding kinetics of an ala-based peptide are slowed by the binding of ions to peptide charged groups.[42]

The 0.8 M $NaClO_4$ AmII′ band normalized intensity time dependence is not well fit to a single exponential, presumably because the extended conformation and α-helix-like conformations have different exchange rates. The double exponential fit to $1-I_{N,AmII'}(t)$

$$1 - I_{N,\,AmII'}(t) = 1 - ae^{-k_1 t} - (1-a)e^{-k_2 t} \tag{3}$$

where $k_1 = 0.022 \pm 0.00$ min^{-1}, $k_2 = 0.00097 \pm 0.0012$ min^{-1}, and $a = 0.77 \pm 0.04$.

The amide NH exchange rate obtained from the excellent single exponential fit to the $C_\alpha-H$ b band exchange kinetics is $k = 0.024$ min^{-1}, which is very close to the k_1 rate obtained from the AmII′ band kinetics. This similarity suggests that the k_1 kinetics derives from the D/H exchange of the extended conformations, leaving the k_2 kinetics to derive from the α-helix-like conformations.

Assuming we have only extended and α-helix-like conformations, we expect parameter a to be given as

$$a = \frac{\sigma_{\text{extended}} f_{\text{extended}}}{\sigma_{\text{extended}} f_{\text{extended}} + \sigma_{\text{helix}} f_{\text{helix}}} \tag{4}$$

where $f_{extended}$ and f_{helix} are the PLL fraction of extended and α-helix-like conformations in the presence of 0.8 M $NaClO_4$. σ_{helix} and $\sigma_{extended}$ are the AmII′ band cross sections of the α-helix-like and extended conformations.

Assuming that the Raman cross sections of the extended and α-helix-like conformations are identical in the presence and absence of $NaClO_4$, $\sigma_{extended}/\sigma_{helix}$ can be estimated from the measured pH ~ 3 PLL UVRR AmII′ band intensities in D_2O in the absence and presence of 0.8 M $NaClO_4$ (Figure 7). Using the AmI′ band as an internal intensity standard, the measured AmII′ band integrated intensity ratio in the absence and presence of 0.8 M $NaClO_4$, $I_{AmII',0MClO4}/I_{AmII',0.8MClO4}$, is measured to be 1.78 ± 0.05. Since

$$\frac{I_{\text{AmII}',\,0\text{MClO}_4}}{I_{\text{AmII}',\,0.8\text{MClO}_4}} = \frac{f_{\text{extended},\,0\text{MClO}_4}\sigma_{\text{extended, AmII}'} + f_{\text{helix},\,0\text{MClO}_4}\sigma_{\text{helical, AmII}'}}{f_{\text{extended},\,0.8\text{ClO}_4}\sigma_{\text{extended, AmII}'} + f_{\text{helix},\,0.8\text{MClO}_4}\sigma_{\text{helical, AmII}'}} \tag{5}$$

Given that our determined PLL extended conformational fractions at 0.0 and 0.8 M $NaClO_4$ are 100% and 28%, we

dx.doi.org/10.1021/jp208918n |J. Phys. Chem. B 2012, 116, 1134–1142

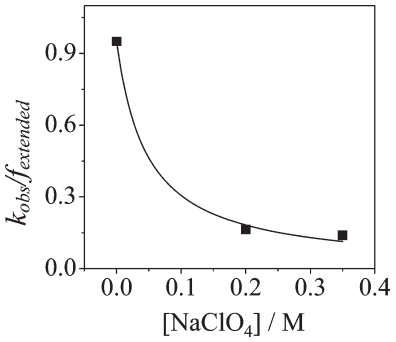

Figure 11. $NaClO_4$ concentration dependence of extended PLL exchange rates. The solid line shows the eq 6 fitting result.

estimate the AmII′ band Raman cross section ratio of the extended conformation to the α-helix-like conformation as 2.55 ± 0.15. Using this cross section ratio and eq 4, we calculate $a = 0.50 \pm 0.02$, which is somewhat less than that of the fitted kinetic result (0.77). This indicates that our two-state H/D exchange model fails to fully account for the PLL exchange kinetics.

$NaClO_4$ Decreases the H/D Exchange Rates of Extended Conformation Peptide Bonds. Figure 11, which shows the $NaClO_4$ concentration dependence of the exponential exchange rates, shows that increasing $NaClO_4$ concentrations rapidly decreases the H/D exchange rate of the peptide bond ND. We can model this dependence at 0, 0.2, and 0.35 M $NaClO_4$ concentrations where the conformational exchange rates are fast by assuming that ClO_4^- is a competitive inhibitor of the PLL H/D exchange. In the Appendix we calculate the impact of ClO_4^- binding on the extended PLL D/H exchange rate by modeling our observed exchange rate, k_{obs}, of Figure 11

$$\frac{k_{obs}}{f_{extended}} = \frac{k_{ex}}{1 + K[ClO_4^-]} \qquad (6)$$

Fitting the apparent exchange rate constant, k_{obs}, at different $NaClO_4$ concentrations (Figure 11) gives an intrinsic D/H exchange rate of $k_{ex} = 0.95 \pm 0.03$ and a ClO_4^- association equilibrium constant to extended PLL of $K = 21 \pm 4\ M^{-1}$. Thus, ClO_4^- binds to extended PLL at a site close to the peptide bond N−D to protect it against D/H exchange that is primarily catalyzed by OH^-. This base-catalyzed reaction occurs through abstraction of the amide NH by direct interaction with OH^-.[43] The model above predicts that increasing the pH should speed up the D/H exchange rate because of an increased competing OH^- concentration. We find that the D/H exchange of PLL at pH 6.5 in 0.8 M $NaClO_4$ is faster than the dead time of our exchange measurement (<1 min); the pH 6.5 in 0.8 M $NaClO_4$ PLL UVRR is identical to that at pH 2.8, indicating identical PLL conformations.

The ClO_4^--induced decrease in the peptide bond NH exchange rates in the extended PLL conformations indicates a specific ClO_4^- binding geometry that protects the backbone peptide bond ND from exchange. Figure 12 shows how the ClO_4^- ion could interact with both an extended conformation peptide bond ND and the neighboring lysine $-NH_3^+$ group through hydrogen bonding and electrostatic interactions to transiently form stable ring structures that protect the amide NH from exchange.

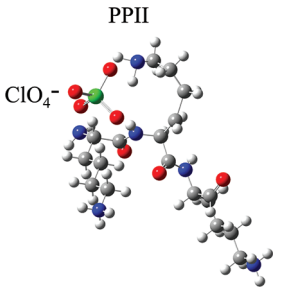

Figure 12. Interactions between ClO_4^- and PLL in the PPII conformation to protect the peptide NH from exchange. The ClO_4^- ion binds to the amide NH and neighboring lysine $-NH_3^+$ group to form a ring structure.

CONCLUSIONS

We examined the impact of $NaClO_4$ on the poly-L-lysine's conformational equilibrium and its hydrogen exchange kinetics. The presence of $NaClO_4$ induces charged PLL to fold into α-helical-like conformations. Extended conformations such as the PPII and 2.5_1-helix conformations dominate the PLL equilibria at low $NaClO_4$ concentrations. In contrast, at higher $NaClO_4$ concentrations α-helical-like conformations that consist of turn, α-helix, and π-helix/bulge conformations dominate. The conformational population Ψ angle distribution and the Gibbs free energy landscapes of PLL were calculated along the Ramachandran Ψ angle folding coordinate.

We find that the D/H exchange kinetics of PLL at 0, 0.2, 0.35, and 0.8 M $NaClO_4$ concentrations slows as the $NaClO_4$ concentration increases. The kinetics of the AmII′ and C_α−H b bands are identical at 0, 0.2, and 0.35 M $NaClO_4$ concentrations which indicates that the conformational interconversion rates are significantly faster than our H/D exchange measurement time scale.

At 0.8 M $NaClO_4$ concentration, the AmII′ band intensity kinetics requires a double exponential fit. In addition, the C_α−H b band extended structure D/H kinetics are faster than that of the AmII′ band indicating that the PLL conformational interconversion rate is slowed by $NaClO_4$. The exchange rate of the extended structure is much faster than that of the α-helix structure. These results allow us to determine the association constant of perchlorate to the extended PLL conformation and allow us to propose a binding geometry.

APPENDIX

$NaClO_4$ Inhibits H/D Exchange of Extended PLL at Low pH. Our results in Figure 11 that show a slowing H/D exchange rate as the ClO_4^- concentration increases indicate that the deuterated amide ND peptide bonds in PLL are protected from exchange by binding of ClO_4^- and PLL to form the ND−ClO_4 complexes. The exchange process of the extended conformations is described by

$$ND - ClO_4 \underset{k_a}{\overset{k_{-a}}{\rightleftarrows}} ND + ClO_4^- \overset{k_{ex}}{\rightleftarrows} NH$$

$$+ ClO_4^- \underset{k_{-a}}{\overset{k_a}{\rightleftarrows}} NH - ClO_4$$

The first and third steps are the association reactions that occur between extended conformations of PLL and ClO_4^-, where k_a

and k_{-a} are the association and dissociation rate constants. k_{ex} is the D to H exchange rate constant. The ClO_4^- association and dissociation steps are very fast, and the reaction is assumed to be in ClO_4^- exchange equilibrium.

The equilibrium association reaction constant between extended PLL and ClO_4^- is

$$K = \frac{k_a}{k_{-a}} = \frac{[ND - ClO_4]}{[ND][ClO_4^-]} \quad (A1)$$

So that

$$[ND - ClO_4] = K[ND][ClO_4^-] \quad (A2)$$

$$[ND - ClO_4] + [ND] = K[ND][ClO_4^-] + [ND] \quad (A3)$$

$$[ND] = \frac{[ND] + [ND - ClO_4]}{1 + K[ClO_4^-]} \quad (A4)$$

During the H/D exchange process, at low and modearate ClO_4^- concentrations (0.2 and 0.35 M), we can assume fast conformational exchange such that the extended and α-helix-like conformations are in equilibrium. Thus, the extended conformational fraction is

$$f_{extended} = \frac{[ND] + [ND - ClO_4]}{[ND] + [ND - ClO_4] + [\alpha - D] + [\alpha - D - ClO_4]} \quad (A5)$$

where $[\alpha-D]$ and $[\alpha-D-ClO_4]$ are the unbound and bound ClO_4^- states of α-helix-like conformations. The measured overall hydrogen exchange rate is

$$-\frac{d([ND] + [ND - ClO_4] + [\alpha - D] + [\alpha - D - ClO_4])}{dt} = k_{ex}[ND] \quad (A6)$$

The hydrogen exchange rate of the extended conformation is obtained from eq A6

$$-\frac{d([ND] + [ND - ClO_4])}{dt} = f_{extended}k_{ex}[ND] \quad (A7)$$

Substituting eq A4 into A7 yields

$$-\frac{d([ND] + [ND - ClO_4])}{dt} = f_{extended}k_{ex}\frac{[ND] + [ND - ClO_4]}{1 + K[ClO_4^-]} \quad (A8)$$

Reorganizing A8

$$-\frac{d([ND] - [ND - ClO_4])}{[ND] - [ND - ClO_4]} = \frac{f_{extended}k_{ex}}{1 + K[ClO_4^-]}dt \quad (A9)$$

Thus, the apparent exchange rate constant of the extended conformation is a function of the ClO_4^- concentration

$$k_{obs} = \frac{f_{extended}k_{ex}}{1 + K[ClO_4^-]} \quad (A10)$$

Rearrange eq A10, and eq 6 is obtained.

AUTHOR INFORMATION

Corresponding Author

*E-mail: asher@pitt.edu. Tel.: (412)-624-8570. Fax: (412)-624-0588.

ACKNOWLEDGMENT

This work is supported by NIH Grant No. 1R01EB009089.

REFERENCES

(1) Baldwin, R. L.; Rose, G. D. *Trends Biochem. Sci.* **1999**, *24*, 26.
(2) Creighton, T. E., *Protein Structure*, 2nd ed.; W.H. Freeman: New York, 1997.
(3) Dill, K. A. *Biochemistry* **1985**, *24*, 1501.
(4) Dill, K. A. *Protein Sci.* **1999**, *8*, 1166.
(5) Dobson, C. M.; Sali, A.; Karplus, M. *Angew. Chem., Int. Ed.* **1998**, *37*, 868.
(6) Dill, K. A.; Ozkan, S. B.; Shell, M. S.; Weikl, T. R. *Annu. Rev. Biophys.* **2008**, *37*, 289.
(7) Anfinsen, C. B. *Science* **1973**, *181*, 223.
(8) Anfinsen, C. B.; Scheraga, H. A. *Adv. Protein Chem.* **1975**, *29*, 205.
(9) Haber, E.; Anfinsen, C. B. *J. Biol. Chem.* **1962**, *237*, 1839.
(10) Levinthal, C. *J. Chim. Phys* **1968**, *65*, 44.
(11) Royer, C. A. *Chem. Rev.* **2006**, *106*, 1769.
(12) Gruebele, M. *Annu. Rev. Phys. Chem.* **1999**, *50*, 485.
(13) Ervin, J.; Sabelko, J.; Gruebele, M. *J. Photochem. Photobiol. B* **2000**, *54*, 1.
(14) Amunson, K. E.; Ackels, L.; Kubelka, J. *J. Am. Chem. Soc.* **2008**, *130*, 8146.
(15) Barth, A.; Zscherp, C. *Q. Rev. Biophys.* **2002**, *35*, 369.
(16) Buchner, G. S.; Murphy, R. D.; Buchete, N. V.; Kubelka, J. *Biochim. Biophys. Acta, Proteins Proteomics* **2011**, *1814*, 1001.
(17) Borgia, A.; Williams, P. M.; Clarke, J. *Annu. Rev. Biochem.* **2008**, *77*, 101.
(18) Schuler, B. *ChemPhysChem* **2005**, *6*, 1206.
(19) Schuler, B.; Lipman, E. A.; Eaton, W. A. *Nature* **2002**, *419*, 743.
(20) Rhoades, E.; Gussakovsky, E.; Haran, G. *Proc. Natl. Acad. Sci. U. S.A.* **2003**, *100*, 3197.
(21) Cecconi, C.; Shank, E. A.; Bustamante, C.; Marqusee, S. *Science* **2005**, *309*, 2057.
(22) Suarez, M.; Jaramillo, A. *J. R. Soc. Interface* **2009**, *6*, S477.
(23) Morra, G.; Meli, M.; Colombo, G. *Curr. Protein Pept. Sci.* **2008**, *9*, 181.
(24) Thirumalai, D.; O'Brien, E. P.; Morrison, G.; Hyeon, C. *Annu. Rev. Biophys.* **2010**, *39*, 159.
(25) Dearborn, D. G.; Wetlaufer, D. B. *Biochem. Biophys. Res. Commun.* **1970**, *39*, 314.
(26) Painter, P. C.; Koenig, J. L. *Biopolymers* **1976**, *15*, 229.
(27) Ma, L.; Ahmed, Z.; Mikhonin, A. V.; Asher, S. A. *J. Phys. Chem. B* **2007**, *111*, 7675.
(28) Bykov, S.; Lednev, I.; Ianoul, A.; Mikhonin, A.; Munro, C.; Asher, S. A. *Appl. Spectrosc.* **2005**, *59*, 1541.
(29) Lednev, I. K.; Karnoup, A. S.; Sparrow, M. C.; Asher, S. A. *J. Am. Chem. Soc.* **1999**, *121*, 8074.
(30) Ma, L.; Ahmed, Z.; Asher, S. A. *J. Phys. Chem. B* **2011**, *115*, 4251.
(31) Mikhonin, A. V.; Myshakina, N. S.; Bykov, S. V.; Asher, S. A. *J. Am. Chem. Soc.* **2005**, *127*, 7712.
(32) Ebert, G.; Kuroyanagi, Y. *Polymer* **1982**, *23*, 1147.
(33) Ebert, G.; Kuroyanagi, Y. *Polymer* **1982**, *23*, 1154.
(34) Goto, Y.; Takahashi, N.; Fink, A. L. *Biochemistry* **1990**, *29*, 3480.
(35) Woody, R. W. In *Circular Dichroism and the Conformational Analysis of Biomolecules*; Fasman, G. D., Ed.; Plenum Press: New York, 1996; p 25.
(36) Reed, J.; Reed, T. A. *Anal. Biochem.* **1997**, *254*, 36.
(37) Ozdemir, A.; Lednev, I. K.; Asher, S. A. *Biochemistry* **2002**, *41*, 1893.

(38) Mikhonin, A. V.; Bykov, S. V.; Myshakina, N. S.; Asher, S. A. *J. Phys. Chem. B* **2006**, *110*, 1928.
(39) Asher, S. A.; Ianoul, A.; Mix, G.; Boyden, M. N.; Karnoup, A.; Diem, M.; Schweitzer-Stenner, R. *J. Am. Chem. Soc.* **2001**, *123*, 11775.
(40) Asher, S. A.; Mikhonin, A. V.; Bykov, S. B. *J. Am. Chem. Soc.* **2004**, *126*, 8433.
(41) Dzubiella, J. *J. Phys. Chem. B* **2010**, *114*, 7098.
(42) von Hansen, Y.; Kalcher, I.; Dzubiella, J. *J. Phys. Chem. B* **2010**, *114*, 13815.
(43) Dempsey, C. E. *Prog. Nucl. Magn. Reson. Spectrosc.* **2001**, *39*, 135.